Particle Accelerators, 1985, Vol. 18, pp. 41–62
0031–2460/85/1801–0041/$25.00/0

THEORETICAL AND EXPERIMENTAL INVESTIGATION OF THE INTERACTION IMPEDANCES AND *Q* VALUES OF THE ACCELERATING CELLS IN THE ADVANCED TEST ACCELERATOR†

R. J. Briggs, D. L. Birx, G. J. Caporaso and V. K. Neil

Lawrence Livermore National Laboratory, University of California, Livermore, CA 94550

and

T. C. Genoni

United States Military Academy, West Point, NY 10996

(*Received Feb. 15, 1985*)

Measured values of the interaction impedance and *Q* values for electromagnetic resonances in the accelerating cells of the Advanced Test Accelerator (ATA) are presented and techniques employed to dampen the resonances are briefly described. The main thrust of this work is the mathematical model of the cells used to treat the resonances analytically. Both azimuthally symmetric (TM_{0n0}) modes and beam-breakup (TM_{1n0}) modes are treated. Agreement between measured values and those predicted by the model is good for the TM_{130} mode, which is the only mode observed to drive the beam-breakup instability in ATA. The values are consistent with observed beam behavior in the accelerator. The analytic treatment predicts a shunt impedance of 60 Ω and a *Q* of 5 for the predominant TM_{0n0} mode. Measurement of the shunt impedance of the TM_{0n0} was not made, but the predicted *Q* value is in good agreement with measurement. Analytic calculations indicate that the damping techniques resulted in *Q* values and interaction impedances that are near optimum for the geometry of the accelerating cells.

INTRODUCTION

Theoretical and experimental investigation of the electromagnetic interaction between the electron beam and the accelerating cells in the Experimental Test Accelerator (ETA) began in 1980. Earlier theoretical efforts had treated the interaction with the azimuthally varying TM_{1n0} modes (so called Beam-Breakup modes).[1] This work provided necessary criteria for the electromagnetic characteristics of the cells in order for the beam-breakup instability to be tolerable in the

† Work performed jointly under the auspices of the U.S. Department of Energy by Lawrence Livermore Laboratory under contract W-7405-ENG-48 and for the Department of Defense under Defense Advanced Research Projects Agency ARPA Order No. 4395 Amendment No. 31, monitored by Naval Surface Weapons Center under document number N60921-84-WR-W0080.

Advanced Test Accelerator (ATA). These criteria are in the form of upper limits on the coupling impedance and the quality factor Q of the cells.

Not much thought was given to possible unstable coherent transverse motion in ETA. As is generally the situation with instabilities in accelerators, this high-frequency unstable motion was first observed experimentally. The observed motion was not so severe as to disrupt the beam, but did provide an opportunity for intense study of the phenomenon in that machine. First of all, extensive microwave measurements were performed on the accelerating cells to find and identify resonant modes.[2] All resonances, azimuthally symmetric ($m = 0$) as well as azimuthally varying, ($m = 1, 2$) in the frequency range of 0 to 850 MHz were investigated and the coupling impedance Z_{t_1} (defined below in Eq. (2.1.1)) and Q value of each $m = 1$ and $m = 2$ mode was determined approximately. (Actually, the values of Z_t/Q and Q were measured). Values of Q ranged from 14 to 70, and values of Z_t/Q for the TM_{1n0} type modes were found to be as high as 12 Ω. With these values measured, it became possible to achieve excellent agreement between experimental data and theoretical calculations.

Theory predicted that values of Z_t and Q as large as those measured would be disastrous if present in the ATA cells. Because of the implications of the phenomenon for the design of ATA, methods were sought and found to reduce the values of Q and Z_t/Q for the accelerating cells.[3] This process is called damping the cells. The damping was accomplished in part by inserting ferrite on conducting surfaces in the cell. For frequencies greater than about 100 MHz, the ferrite is nondispersive and an excellent absorber of electromagnetic energy. The accelerating-voltage pulse was unaffected by the presence of the ferrite. A summary of the damping techniques employed and the experimental observations in ETA is contained in Ref. 4. One of the purposes of this work is to show that damping is near optimum for the cell geometry. These changes were implemented in the existing ETA cells and in the design of the ATA cells. In this work, we often refer to the undamped or damped cell, and the terms correspond to the cell configuration before and after the damping methods were implemented. Some of the measured parameters are given in Table I, which is taken from Refs. 2 and 3.

TABLE I

Parameters of some of the Modes Found Experimentally in the ETA Accelerating Cells. Because of the Symmetry of the Cell, Degeneracy Exists, but only the Branches with Highest Q Value are Listed. The Last Column Lists the Q Values in the Cell with Ferrite but no Corner Reflector

Mode	f(MHz)	Z_t/Q	Q	$Q(D)$
TM_{010}	220		14	10
TM_{110}	345	8.8 Ω	40	5
TM_{020}	535		34	20
TM_{120}	605	10.2 Ω	50	5
TM_{210}	665		45	
TM_{030}	770		70	10
TM_{130}	830	12.2 Ω	60	12

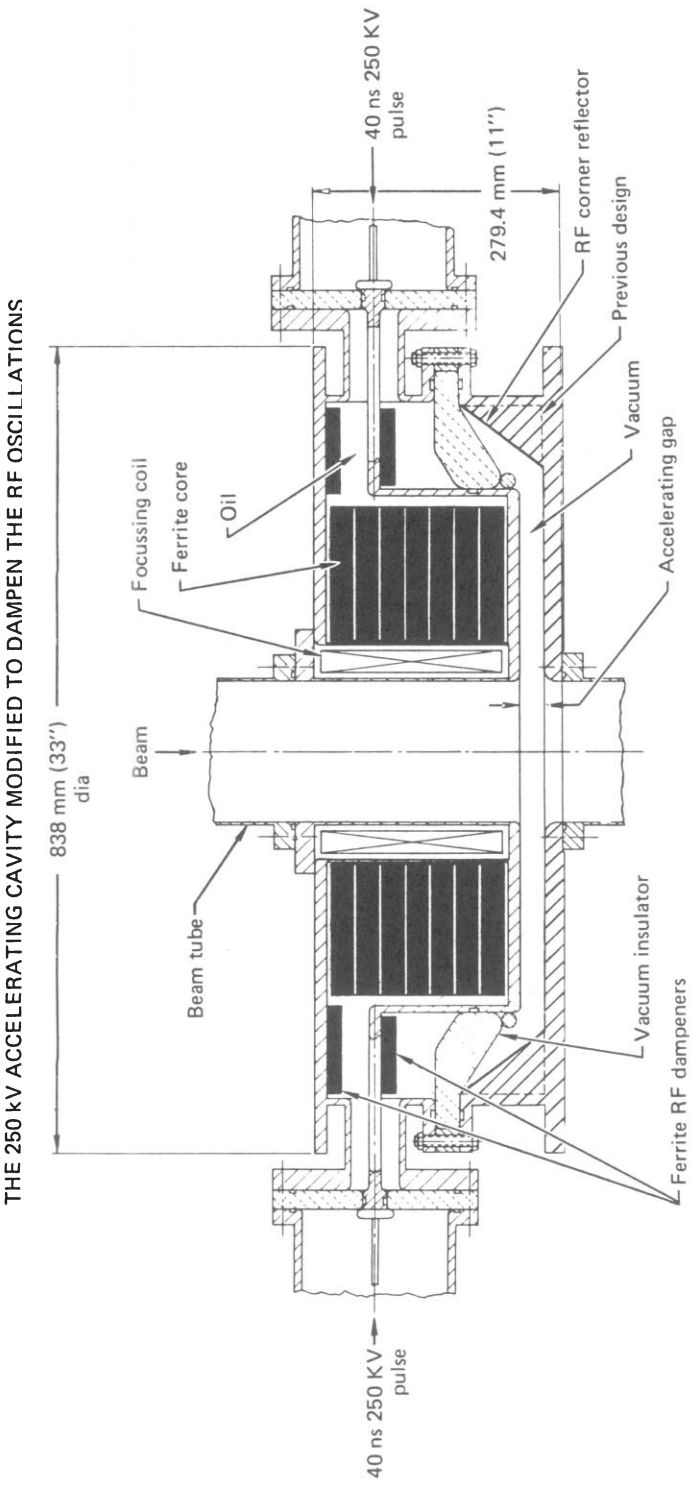

FIGURE 1. The 250 kV accelerating cavity modified to dampen the RF oscillations.

The final damping mechanism employed was the rf corner reflector which can be seen in the ETA cell shown in Fig. 1. The angle was chosen to bring the TM waves into the ceramic insulator at the Brewster Angle and thus enhance transmission through the insulator to the ferrite. The corner reflector further reduced the values of Q by about a factor of 2 from those listed in the last column of Table I.

The measurements suggested a theoretical model of the cells that proved quite useful in further understanding of the beam-breakup phenomenon in ATA. The application of this model to the azimuthally symmetric modes was not pursued until recently. With the almost total suppression of unstable transverse motion in ATA by means of laser guiding, the importance of the theoretical understanding of the beam-breakup phenomenon has been reduced, at least for that machine.[5] However, the work is of sufficient interest and applicability to induction linacs that the investigation will be presented in Section 2.

In Section 1, we describe the theoretical model of the cell. We then present a study of an azimuthally symmetric mode of the cells, and the possible consequences of the electron beam's interaction with this mode. The mathematical treatment is considerably less complicated than that for the asymmetric modes, and offers an introduction to the theoretical model of the cells and the calculational technique.

1. THE TM_{0n0} MODES

Azimuthally symmetric fields in the cells will be excited by the time-dependent current of the beam pulse, and as a result the total voltage on the cells will be time-dependent. If there exists a resonance in the cell (i.e., a characteristic normal mode), the resonance will be excited by the rising current at the head of the beam pulse and a sinusoidal oscillation of cavity voltage will occur. At best, this sinusoidal voltage may cause an undesirable sinusoidal variation in the energy of particles being accelerated. Such a variation (or indeed, any time-dependent energy variation) leads to difficulty in transporting the beam from the accelerator to various experimental areas. A significant sinusoidal variation may even render the beam useless for some experiments. At worst, the sinusoidal energy variation may cause a longitudinal modulation of the beam current that could grow exponentially with distance down the accelerator. This phenomenon may be regarded as the "longitudinal cousin" of the beam-breakup instability. A detailed investigation of this instability is beyond the scope of this work.

1.1 Model of the Cell

The following model is in no way a complete description of the electro-magnetic properties of the accelerating cells in ETA and ATA, but its success in predicting the transverse interactions of the beam and the cells was quite gratifying, as will be discussed in Section 2. The model allows a determination of the appropriate

values of ω_0, Z, and Q without assumptions regarding high values of Q or well-separated normal modes.

Microwave measurements of $m = 0$ (azimuthally symmetric modes) and $m = 1$ (beam-breakup modes) in the ETA cell indicated modes with zeros in the azimuthal magnetic field at the inner radius of the insulator, $r = R$ in Fig. 1. The radius R is 27 cm in these cells. For $m = 1$ modes the, frequencies 345 MHz and 830 MHz (The TM_{110} and TM_{130} modes in Table I) correspond approximately to the first two zeros of $J_1'(\omega R/c)$, where J_1 is the first-order ordinary Bessel function of the first kind, and a prime designates differentiation with respect to the argument. The first two zeros of J_1' are 1.84 are 5.33, and the calculated frequencies are 322 MHz and 950 MHz, respectively. For $m = 0$, there is a mode with frequency 770 MHz (The TM_{030} mode in Table I) corresponding to a zero of $J_0'(\omega R/C)$. This mode had the highest Q value, 70, of all modes found in the undamped cells. The first zero of J_0' is 3.83, and the calculated frequency is 670 MHz. The theoretical model of the cell described below provides better agreement with the measured frequency of the TM_{030} mode.

Physically, there is an impedance at $r = R$ significantly higher than the radial line impedance at that point. Stimulated by this observation, we consider the simple geometry shown in Fig. 2. The radial line is terminated with a resistive surface at $r = R$. This model does not take into account other modes found in the undamped cells, but the three modes that are approximated by our model had the highest Q values in the undamped cell. Furthermore, the $m = 1$ mode at 830 MHz is the only one observed to drive unstable coherent motion of the beam in ETA and ATA.

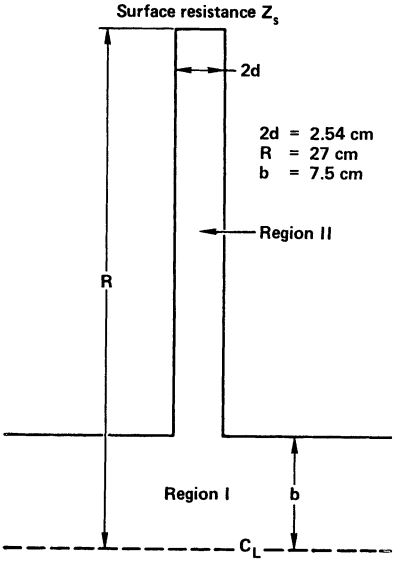

FIGURE 2. Idealized model of the cell. The cylindrical surface at $r = R$ has surface resistance Z_s.

1.2. *Induced Voltage in Terms of Z and Q*

We use a single-mode analysis to define an impedance Z and a quality factor Q. We will determine values for Z and Q in Section 1.4 utilizing our theoretical model of the cell. A time-dependent current $I(t)$ passing through the cell and exciting a resonant mode will create a voltage $V(t)$ across the gap given by

$$V(t) = -\frac{Z}{Q}\int_0^t \frac{dI(t')}{dt'} e^{-\alpha(t-t')} \sin \omega_0(t-t')\, dt'. \tag{1.2.1}$$

In this expression, ω_0 is the resonant frequency and $\alpha = \omega_0/2Q$. We neglect $(1/2Q)^2$ with respect to unity. The beam head enters the cell at $t = 0$. The quantity Z is often called the shunt impedance of the cell and Z/Q is called the surge impedance. An equivalent and more commonly used definition is

$$\frac{Z}{Q} = \frac{V^2}{2\omega_0 U}, \tag{1.2.2}$$

in which V is the voltage on the cell, ω_0 is the resonant frequency, and U is the stored energy in the cell. The definition applies when the particular mode is driven at resonance. Once values for ω_0, Z/Q, and Q are known, the induced voltage $V(t)$ can be found for any $I(t)$. In particular, if we have

$$I(t) = I_0 e^{i\omega t}, \tag{1.2.3}$$

the steady-state voltage is given by

$$V(\omega) = -\frac{i\omega\omega_0 Z I_0 e^{i\omega t}}{Q[(\omega_0^2 - \omega^2) + i(\omega\omega_0/Q)]}. \tag{1.2.4}$$

Equation (1.2.4) is to be used in conjunction with our model of the cell to determine values of ω_0, Z, and Q.

In Section 1.4, we investigate the voltage induced on the cell by a time-dependent beam current and the time dependent particle energy that may result from this voltage. We employ a beam current of the form

$$I = I_b(1 - e^{-\mu t}). \tag{1.2.5}$$

Inserting this expression into Eq. (1.2.1), we find

$$V(t) = -\frac{\mu Z}{Q} I_b \frac{[\omega_0(e^{-\mu t} - e^{-\alpha t}\cos\omega_0 t) + (\mu - \alpha)e^{-\alpha t}\sin\omega_0 t]}{[(\mu-\alpha)^2 + \omega_0^2]}. \tag{1.2.6}$$

1.3. *Electromagnetic Fields of the TM_{0n0} Modes*

We proceed to calculate the voltage induced across the cell shown in Fig. 2 as a function of frequency. We could consider a current on axis varying as $\exp i\omega[t - (z/v)]$ as the source of electromagnetic fields. It turns out to be easier to consider a surface current in the gap (i.e., the surface $r = b, |z| < d$ in Fig. 2) as the source. If the cell were not present and the pipe wall were continuous, a surface current K

would exist in the wall, and the electric and magnetic fields in the pipe are easily obtained. The presence of the cell produces additional contributions to the electromagnetic fields. The source of these additional contributions may be taken as a surface-current $-K$ in the gap. The proper expression for this surface current is derived in Appendix A, and is given by Eq. (A15), which is valid for any particle energy. However, for relativistic electrons, Eq. (A16) suffices. A surface-charge source should also be placed in the gap, but the electric fields from this source would decay exponentially with radius inside the cell.

The procedure we follow is to write down appropriate expressions for the field components in the pipe (region I in Fig. 2) and in the box (region II in Fig. 2). These expressions represent a uniform E_z in the gap. There is one constant that is evaluated by averaging the condition

$$B_\theta^{II} - B_\theta^I = -4\pi K/c \tag{1.3.1}$$

across the gap. Gaussian units are employed, but results are given in practical units. This procedure is equivalent to matching the current and voltage in the two regions. The continuity of the radial electric field E_r is not accomplished by this method. In fact, the details of the field configuration near the "edges" are not properly treated. There are two reasons why this is justified. First, the fields around the edges decay exponentially both inward and outward and do not contribute much to the fields on the pipe axis where the beam is, or to the fields at $r = R$ where the surface impedance is located. The second reason is that in practice the edges are founded in the cells, not square as in our model.

We take the vector potential in the pipe to be

$$\mathbf{A}^I = \frac{A_0}{\pi} e^{i\omega t} \int_{-\infty}^{\infty} \frac{\sin kd}{k} \frac{e^{ikz}}{I_0(qb)} \left[-\frac{ik}{q} I_1(qr)\hat{r} + I_0(qr)\hat{z} \right] dk. \tag{1.3.2}$$

In this expression the quantity q is given by

$$q^2 = k^2 - (\omega/c)^2,$$

and I_0 and I_1 are modified Bessel functions of the first kind of order zero and one, respectively. We note that $\nabla \cdot \mathbf{A} = 0$ and A_z is a solution of the equation

$$\frac{1}{r}\frac{\partial}{\partial r}\left(r\frac{\partial A_z}{\partial r}\right) + \frac{\partial^2 A_z}{\partial z^2} + \frac{\omega^2}{c^2} A_z = 0. \tag{1.3.3}$$

At $r = b$ we have

$$A_z = \begin{cases} A_0 e^{i\omega t}, & |z| < d \\ 0, & |z| > d \end{cases}. \tag{1.3.4}$$

At this cylindrical surface A_z, and thus $E_z = -i(\omega/c)A_z$, is zero outside the gap and uniform in z in the gap.

We consider no z dependence of the fields in the box, so that the vector potential has only an axial component given by

$$A_z^{II} = A_0 G(\omega r/c)/G(\omega b/c). \tag{1.3.5}$$

The form of Eq. (1.3.5) guarantees the continuity of A_z across the gap. Details of

the function G are discussed below. In the box, $B_\theta = -\partial A_z/\partial r$, or

$$B_\theta^{II} = -A_0 \frac{\omega}{c} \frac{G'(\omega r/c)}{G(\omega b/c)}. \tag{1.3.6}$$

In the pipe $B_\theta = (\partial A_r/\partial z) - (\partial A_z/\partial r)$. From Eq. (1.3.2) we obtain

$$B_\theta^I = \frac{A_0}{\pi}\left(\frac{\omega}{c}\right)^2 e^{i\omega t}\int_{-\infty}^{\infty} \frac{\sin kd}{kq} \frac{I_1(qr)}{I_0(qb)} e^{ikz}\, dk. \tag{1.3.7}$$

We insert Eqs. (1.3.6) and (1.3.7) into Eq. (1.3.1) and employ Eq. (A16) to obtain (in the gap only, $|z| < d$),

$$-A_0\left\{\frac{\omega}{c}\frac{G'(\omega b/c)}{G(\omega b/c)} + \frac{1}{\pi}\left(\frac{\omega}{c}\right)^2 \int_{-\infty}^{\infty} \frac{\sin kd}{kq} \frac{I_1(qb)}{I_0(qb)} e^{ikz}\, dk\right\} = \frac{2I}{cb} e^{-i\omega z/v}. \tag{1.3.8}$$

Rather than averaging Eq. (1.3.8) over the gap, we will first greatly simplify the numerical evaluation of A_0 by evaluating the integral by contour integration. There are no branch points in the complex k plane because $I_0(qb)$ is even in q and $I_1(qb)$ is odd in q. We deform the contour to pass below the origin. (It could just as well pass above.) When we write

$$\sin kd e^{ikz} = \frac{1}{2i}[e^{ik(d+z)} - e^{ik(z-d)}],$$

we must close the contour for the first term in the upper half k plane and for the second term in the lower half k plane. Integration of the first term has a contribution from the simple pole at $k = 0$. The residue at the origin is

$$\text{Res}\,(k=0) = \left[\frac{I_1(qb)}{2iqI_0(qb)}\right]_{k=0} \tag{1.3.9}$$

at $k = 0, q^2 = -(\omega/c)^2$. We choose $q = i\omega/c$, although again the choice is of no consequence, and note that

$$I_0(ix) = J_0(x), \qquad I_1(ix) = iJ_1(x),$$

so that

$$\text{Res}\,(k=0) = \frac{c}{2i\omega}\frac{J_1(\omega b/c)}{J_0(\omega b/c)},$$

$$= -\frac{c}{2i\omega}\frac{J_0'(\omega b/c)}{J_0(\omega b/c)}. \tag{1.3.10}$$

There are an infinite number of poles up and down the imaginary k axis corresponding to $q_s = i\beta_s$, where β_s are the roots of $J_0(\beta_s b) = 0$. The values of k at these poles is $k_s^2 = (\omega/c)^2 - \beta_s^2$, and, since the frequencies of interest are below the cutoff frequency of the pipe, ($\omega_c = c\beta_1$), these poles are located at $k_s = \pm i\nu_s$, where

$$\nu_s^2 = \beta_s^2 - (\omega/c)^2. \tag{1.3.11}$$

The residue at one of these poles in the upper half k plane is

$$\text{Res}\,(k = i\nu_s) = \frac{e^{-\nu_s(d+z)}}{2i}\left[\frac{I_1(qb)}{kqdI_0/dk}\right]_{k=i\nu_s} \tag{1.3.12}$$

We have

$$\frac{dI_0(qb)}{dk} = bI_1(qb)\frac{dq}{dk},$$

$$= (bk/q)I_1(qb), \tag{1.3.13}$$

so that Eq. (1.3.12) becomes

$$\text{Res}\,(k = i\nu_s) = -\frac{e^{-\nu_s(d+z)}}{2i\nu_s^2 b}. \tag{1.3.14}$$

Similarly we find, for poles in the lower half k plane,

$$\text{Res}\,(k = -i\nu_s) = -\frac{e^{-\nu_s(d-z)}}{2i\nu_s^2 b}. \tag{1.3.15}$$

We go around these poles in a clockwise direction, but the minus sign in front of this term compensates for that. Finally we have

$$\int_{-\infty}^{\infty} \frac{\sin kd}{kq}\frac{I_1(qb)}{I_0(qb)} e^{ikz}\,dk = 2\pi i \sum \text{Res},$$

$$= -\pi\left\{\frac{c}{\omega}\frac{J_0'(\omega b/c)}{J_0(\omega b/c)} + \frac{2}{b}\sum_s \frac{e^{-\nu_s d}\cosh \nu_s z}{\nu_s^2}\right\}. \tag{1.3.16}$$

We now have an expression devoid of integrals and Bessel functions. We insert Eq. (1.3.16) into Eq. (1.3.8) and average the equation over the gap, $-d < z < d$ to obtain the equation from which we evaluate the quantity A_0. This equation is

$$\frac{\omega A_0}{c} = \frac{2I}{cb}\frac{\sin(\omega d/v)}{(\omega d/v)}\frac{1}{H}, \tag{1.3.17}$$

in which the quantity H is given by

$$H = \frac{J_0'(\omega b/c)}{J_0(\omega b/c)} - \frac{G'(\omega b/c)}{G(\omega b/c)} + \frac{\omega}{cbd}\sum_s \frac{(1 - e^{-2\nu_s d})}{\nu_s^3}. \tag{1.3.18}$$

All the electromagnetic properties of the cell are contained in the function G, and up to this point we could place any complex impedance Z_s on the surface $r = R$. The boundary condition at $r = R$ is

$$E_z = -\frac{Z_s}{Z_0} B_\theta,$$

in which Z_0 is the impedance of free space. The desired function G is given by

$$G = J_0(\omega r/c) + CN_0(\omega r/c), \tag{1.3.19}$$

with C given by

$$C = \frac{[i(Z_s/Z_0)J_0'(\omega R/c) - J_0(\omega R/c)]}{[N_0(\omega R/c) - i(Z_s/Z_0)N_0'(\omega R/c)]}. \tag{1.3.20}$$

In these equations, N_0 is the ordinary Bessel function of the second kind of order zero.

1.4. Determination of Z and Q for the TM_{030} Mode

We calculate the change in kinetic energy of a particle that traverses the cell. This change ΔE is given by

$$\Delta E = e\int E_z\, dz, \tag{1.4.1}$$

in which $E_z = -i(\omega/c)A_z$, and the integral is taken over the particle's path. If the particle passes the center of the cell ($z=0$) at $t=t_0$, this path is $z=v(t-t_0)$, or $t=t_0+(z/v)$. The particle's radial position is assumed to remain constant. Employing Eq. (1.3.2) we have

$$\Delta E = -\frac{i\omega}{c}e\frac{A_0}{\pi}e^{i\omega t_0}\int_{-\infty}^{\infty}\frac{\sin kd}{k}\frac{I_0(qr)}{I_0(qb)}\int_{-\infty}^{\infty}e^{i[k+(\omega/v)]z}\,dz\,dk. \tag{1.4.2}$$

We perform the integral over z first to obtain

$$\frac{1}{\pi}\int_{-\infty}^{\infty}e^{i[k+(\omega/v)]z}\,dz = 2\delta[k+(\omega/v)]. \tag{1.4.3}$$

The integral over k is now trivial, and we obtain

$$\Delta E = -2i\left(\frac{\omega}{c}\right)eA_0\,d\frac{\sin(\omega d/v)}{(\omega d/v)}\frac{I_0(gr)}{I_0(gb)}e^{i\omega t_0}. \tag{1.4.4}$$

As in Appendix A, $g=\omega/v\gamma$ and for relativistic particle energy, $I_0(gr)=I_0(gb)=1$. For non-relativistic particle energy, such as in a heavy-ion beam, this approximation must be reexamined.

We include the additional factor $\sin(\omega d/v)/(\omega d/v)$ in our evaluation of A_0 and introduce the quantity A_0^e by the definition

$$A_0^e = \frac{\sin(\omega d/v)}{(\omega d/v)}A_0. \tag{1.4.5}$$

We numerically determine the function $P(\omega)$, which is defined by

$$\begin{aligned} P(\omega) &= \frac{\sin^2(\omega d/v)}{(\omega d/v)^2}\frac{1}{H} \\ &= \left(\frac{\omega A_0^e}{c}\right)\left(\frac{cb}{2I}\right). \end{aligned} \tag{1.4.6}$$

We have evaluated the quantity $P(\omega)$ for values $b=7.5$ cm (for the ETA cell) and $b=6.7$ cm (for the ATA cell). The difference is inconsequential and we present only the results for the ETA cell. Only the imaginary part of P enters in determining values of Z and Q. Graphs of Im $P(\omega)$ vs $\omega R/c$ are shown in Figs. 3, 4, and 5a for $Z_s/Z_0=1$, 2, and 3 respectively. These values of Z_s/Z_0 are chosen

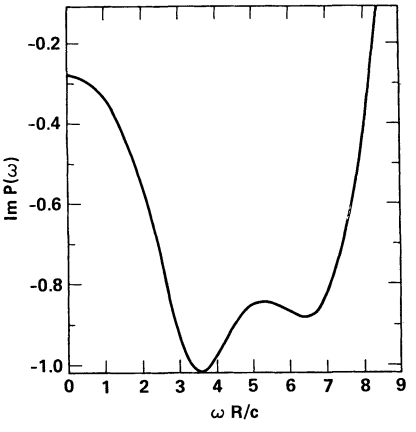

FIGURE 3. Imaginary portion of $P(\omega)$ defined by Eq. (1.4.6) vs $\omega R/c$ for $Z_s = Z_0$.

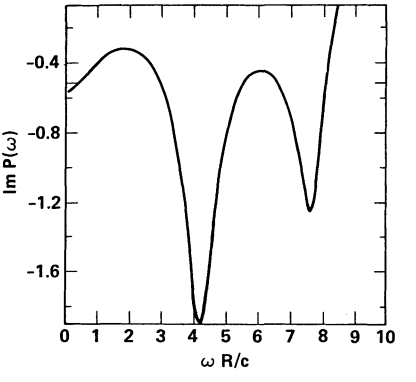

FIGURE 4. Imaginary portion of $P(\omega)$ defined by Eq. (1.4.6) vs $\omega R/c$ for $Z_s = 2Z_0$.

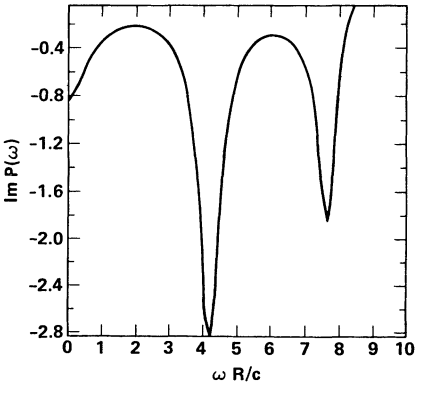

FIGURE 5a. Imaginary portion of $P(\omega)$ defined by Eq. (1.4.6) vs $\omega R/c$ for $Z_s = 3Z_0$.

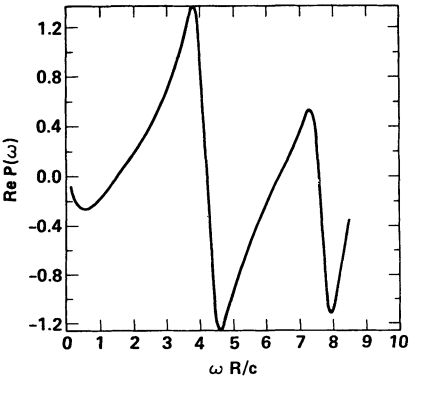

FIGURE 5b. Real portion of $P(\omega)$ defined by Eq. (1.4.6) vs $\omega R/c$ for $Z_s = 3Z_0$.

for comparison with measured parameters in the damped cell. The curves extend to $\omega R/c = 8.6$, which corresponds to the cutoff frequency of the beam pipe given by $\omega b/c = 2.405$. For $b = 7.5$ cm, the cutoff frequency is 1530 MHz. The real part of $P(\omega)$ for $Z_s/Z_0 = 3$ is plotted in Fig. 5b, and is seen to be zero at values of $\omega R/c$ corresponding to peaks in Im P.

All three of the plots of Im P exhibit two peaks. For $Z_s/Z_0 = 2$ and 3, the peaks occur at $\omega R/c = 4.2$ and 7.6. A detailed examination of the function H in Eqs. (1.3.18) shows that these peaks occur at values of $\omega R/c$ slightly greater than the second and third zeros of $N_0(\omega R/c)$. These zeros are 3.96 and 7.09. The peak at $\omega R/c = 4.2$ corresponds to a frequency of 743 MHz, in remarkable agreement with the measured value for the TM_{030} mode. (It should be mentioned that this mode was two-fold degenerate, and the frequency of the other branch had a

measured value of 735 MHz.) The second peak at $\omega R/c = 7.6$ corresponds to a frequency above the range of measurement. If this mode is present in the cell, its coupling to the beam is less than that for the TM_{030}, so the latter should be the dominant mode.

For the "matched" condition, $Z_s = Z_0$ in Fig. 3, the peaks occur at lesser values of $\omega R/c$, as is expected since the values of Q are so low that $(1/2Q)^2$ is not small compared with unity as we will see below.

Comparison with measured parameters in the undamped cell is of little interest, but it was found that a value of Z_s/Z_0 of 10 in our model gave a Q value of 50. The frequencies at the peaks of Im P remain the same as in Figs. 4 and 5a.

We proceed to evaluate Z and Q from the graphs of Im P and Eq. (1.2.4). At resonance, Eq. (1.2.4) yields $V = -ZI$. Also we have $V = -2id\omega A_0^e/c$, and at resonance ($\omega = \omega_0$) Re $A_0 = 0$ so that

$$ZI = -2d(\omega/c)\ \text{Im}\ A_0^e(\omega_0) \tag{1.4.7}$$

Employing Eq. (1.4.6) we obtain

$$Z = -(4d/cb)\ \text{Im}\ P(\omega_0).$$

In Gaussian units $Z_0 = 4\pi/c$, so that, independent of units,

$$(Z/Z_0) = -(d/\pi b)\ \text{Im}\ P(\omega_0). \tag{1.4.8}$$

For the ETA cells $d/\pi b = 5.4 \times 10^{-2}$. From the graphs, Fig. 3 through 5, we calculate the values of Z shown in Table II.

TABLE II

Values of Z and Q for the TM_{030} as Estimated from Theoretical Model of the ETA Accelerating Cell

Z_s/Z_0	$Z(\Omega)$	Q
1	22.4	2.3
2	38	3.1
3	57	5.3

We estimate the values of Q from the behavior of Im P near resonance. In Eq. (1.2.4) we use the approximations $\omega_0^2 - \omega^2 = 2\omega_0(\omega_0 - \omega)$ and $\omega\omega_0/Q = \omega_0^2/Q$, and obtain

$$\text{Re}\ V(\omega) = \text{Re}\ V(\omega_0)\left(\frac{\omega_0}{2Q}\right)^2 \frac{1}{[(\delta\omega)^2 + (\omega_0/2Q)^2]}, \tag{1.4.9}$$

in which Re $V(\omega_0) = -ZI$, and $\delta\omega = \omega_0 - \omega$. Since Re $V \propto$ Im P, we solve Eq. (1.4.9) for Q and obtain

$$Q = \frac{1}{2}\frac{\omega_0}{\delta\omega}\left[\frac{\text{Im}\ P(\omega_0)}{\text{Im}\ P(\omega)} - 1\right]^{1/2}. \tag{1.4.10}$$

For $Z_s/Z_0 = 2$, and 3, it is easy to estimate Q from the graphs and Eq. (1.4.10). For $Z_s/Z_0 = 1$, the estimate is less firm. Values of Z and Q are given in Table II.

So far the greatest success of our model is the prediction of the frequency of the TM_{030} mode. The impedances Z of the azimuthally symmetric modes were not measured. The Q values were measured, and for $Z_s/Z_0 = 3$, our prediction of $Q = 5.3$ is consistent with measurements in the cell with ferrite and *rf* corner reflector. From Table II we see that Z/Q is relatively independent of Z_s/Z_0, as it should be. The significant result of these calculations is that for a matched impedance $Z_s = Z_0$, the Q value is somewhat lower than for higher values of Z_s, but Z/Q is not very different, and we conclude that no amount of damping in the cells will appreciably reduce Z/Q from a value of about 12 Ω. The only way to further reduce Z/Q would be to taper the radial line so that the cells are sections of a sphere.

For $Z/Q = 12\ \Omega$ and $Q = 5$, we have calculated the induced voltage given by Eq. (1.2.6). For the TM_{030} mode, we have $\omega_0 = 4.2c/R = 4.7\ (\text{nsec})^{-1}$ and $\alpha = \omega_0/2Q = 0.47\ (\text{nsec})^{-1}$. If we choose a 10 to 90% current rise time of 10 nsec, $\mu = 0.22\ (\text{nsec})^{-1}$. With these parameter values, Eq. (1.2.6) may be approximated by

$$V(t) = -I_b \frac{\mu Z}{\omega_0 Q} (e^{-\mu t} - e^{-\alpha t} \cos \omega_0 t). \tag{1.4.11}$$

For a beam current $I_b = 10$ kA, the coefficient is 5.6 kV. The time-dependent factor in the parenthesis reaches a peak value of 1.6 at $\omega_0 t \sim \pi$, but decays with an e-folding time of 10 nsec. The applied accelerating voltage on the cell is 250 kV, so that the induced voltage will result in a few percent energy modulation of particles in the front portion of the beam. As of this writing, there are no direct experimental measurements of particle energy at the end of ATA, but beam transport generally improves with slower current rise.

2. THE TM_{1n0} MODES

In this section, we use our model of the cell to obtain values of Z_t and Q to compare with the measured values given in Table I. The interaction of the beam with these modes (in particular the TM_{130} mode) results in unstable coherent transverse oscillations of the beam. This instability (commonly known as the beam-breakup instability) has been investigated experimentally and computationally in both ETA and ATA. The data can be compared with computational results to verify values of Z_t and Q for the accelerating cells.

Although the theory of Ref. 1 is not strictly applicable to ATA, it can be used to illustrate how these values can be determined. In Ref. 1 the quantity $k \equiv \omega Z_t/Q$, with Z_t in sec/cm. (The units are unimportant in this discussion.) Under conditions satisfied in ATA, the amplitude of transverse oscillations at the nth accelerating cell reaches its peak value at a time t_m given by Eq. (5.15) of Ref. 1,

$$t_m = 2nZ_tQ\rho I/I_a.$$

In this relation, t is measured from the time the head of the beam (or the initial perturbation) passes the nth cell. The beam current is I, $I_a = 17\gamma\beta$ kA, and

$\rho = \gamma\beta mc^2/B_s$, with B_s the magnitude of the solenoidal guide field in the accelerator. The peak value of the amplitude at the nth cell at time t_m is $\xi_0 \exp \Gamma_m$, where ξ_0 is the initial perturbation amplitude and Γ_m is given by Eq. (5.14) of Ref. 1,

$$\Gamma_m = nZ_t\omega\rho I/I_a.$$

Both t_m and Γ_m can be obtained from experiment, giving separate measurements of Z_t and Q. The values obtained from experiment and computation may be regarded as values measured by the beam in the actual accelerator, as contrasted to those measured in cold tests and presented in Table I. The two sets of measured values are in reasonably good agreement.

2.1. *Transverse Impulse in Terms of Z_t and Q*

In crossing the cell, a particle will undergo a change in transverse momentum proportional to $\int B_y\, dz$ along its trajectory. Analogous to Eq. (1.2.2), we introduce a transverse coupling impedance Z_t by the definition

$$\frac{Z_t}{Q} = \frac{[\int B_y\, dy]^2}{2\omega_0 U}, \tag{2.1.1}$$

where again the definition applies for the mode driven at the resonance frequency ω_0, and U is the stored energy in the mode. In Gaussian units $B_y\, dz$ has dimensions of a voltage, and for brevity we introduce the quantity V_t given by the definition

$$V_t(\omega) = \int B_y(\omega)\, dz, \tag{2.1.2}$$

which now holds for the cell driven at any frequency. Equation (2.1.1) is equivalent to the definition of Z_t in Ref. 1.

The TM_{1n0} modes of the cell are driven by a current I displaced a distance ξ from the axis of the cell. Either or both I and ξ may be time-dependent. If, as in Section I, we take the time dependence of the product $I\xi$ to be $e^{i\omega t}$, the equation analagous to Eq. (1.2.4) is

$$V_t(\omega) = \frac{\omega_0^3}{cQ} \frac{Z_t I\xi e^{i\omega t}}{[(\omega_0^2 - \omega^2) + i(\omega\omega_0/Q)]}. \tag{2.1.3}$$

In Section 2.3, we shall determine values of Z_t and Q from our model of the cell and compare these values to the measured values in Table I.

2.2. *Electromagnetic Fields for TM_{1n0} Modes*

We again replace the beam with a surface-current source in the gap. In the absence of the gap, there would be a wall current in the z direction, which we label K_t. The beam in ETA is focused with a solenoidal magnetic field, and the

transverse coherent motion of the beam is complicated, so the resulting wall current is also complicated. In fact, the wall current also has an azimuthal component. However, if the frequency of transverse (i.e., betatron) motion is much less than the frequencies of interest in the cell ($\approx$800 MHz), to a good approximation we may neglect the focusing in this treatment. We choose a beam with current constant in time, and oscillating in the x direction with a displacement from the pipe axis given by $\xi \exp i\omega[t-(z/v)]$. The wall current K_t is found in Appendix B and given by Eq. (B7). For relativistic particle energy, the approximate expression in Eq. (B8) suffices.

The expressions for the vector potential $\mathbf{A}$ in the pipe and in the box are chosen so that E_z and B_r are uniform in the gap, and $E_\theta = 0$ on the surface $r = b$. The vector potential is more complex than that in Section 1, because both transverse electric and transverse magnetic fields are needed to satisfy the boundary conditions. The axial component A_z must satisfy the equation

$$\left[\frac{1}{r}\frac{\partial}{\partial r}\left(r\frac{\partial}{\partial r}\right)+\frac{1}{r^2}\frac{\partial^2}{\partial\theta^2}+\frac{\partial^2}{\partial z^2}+\frac{\omega^2}{c^2}\right]A_z = 0. \tag{2.2.1}$$

We consider the following expressions for $\mathbf{A}$ in the pipe. (The superscript I is omitted for neatness.)

$$\mathbf{A}^{TM} = \frac{A_1}{\pi} e^{i\omega t}\int_{-\infty}^{\infty} \frac{\sin kd}{I_1(qb)} e^{ikz} \times\left\{-\frac{i}{q}\left[\cos\theta I_1'(qr)\hat{r} - \sin\theta\frac{I_1(qr)}{qr}\hat{\theta}\right]+\cos\theta\frac{I_1(qr)}{k}\right\} dk \tag{2.2.2}$$

$$\mathbf{A}^{TE} = \frac{iA_1}{\pi b} e^{i\omega t}\int_{-\infty}^{\infty} \frac{\sin kde^{ikz}}{q^2 I_1'(qb)}[\cos\theta I_1(qr)\hat{r} - \sin\theta I_1'(qr)\hat{\theta}]\, dk. \tag{2.2.3}$$

We note that A_z satisfies Eq. (2.2.1) and $\nabla\cdot\mathbf{A}^{TM} = \nabla\cdot\mathbf{A}^{TE} = 0$. On the surface $r = b$ we have $A_\theta = 0$, and

$$A_z = \begin{cases} A_1\cos\theta e^{i\omega t} & |z|<d. \\ 0 & |z|>d \end{cases} \tag{2.2.4}$$

Both $E_z = -i\omega A_z/c$ and $B_r = \partial A_z/r\,d\theta$ are uniform in the gap. The constant A_1 will be chosen again by averaging the condition

$$B_\theta^{II} - B_\theta^{I} = -4\pi K_t/c, \tag{2.2.5}$$

across the gap. The continuity of E_r and B_z cannot be satisfied by these expressions, but this shortcoming is ignored for the reasons stated in Section 1.

From Eqs. (2.2.2) and (2.2.3) we calculate B_θ, which is given by

$$B_\theta = \frac{\partial A_r}{\partial z} - \frac{\partial A_z}{\partial r}.$$

On the surface $r = b$, the expressions for B_θ^{TM} and B_θ^{TE} are

$$B_\theta^{TM}(r=b) = \left(\frac{\omega}{c}\right)^2\frac{A_1}{\pi}\cos\theta e^{i\omega t}\int_{-\infty}^{\infty}\frac{\sin kd}{kq} e^{ikz}\frac{I_1'(qb)}{I_1(qb)}\, dk, \tag{2.2.6}$$

and

$$B_\theta^{TE}(r=b) = -\frac{A_1}{\pi b^2}\cos\theta e^{i\omega t}\int_{-\infty}^{\infty} k\sin kd e^{ikz}\frac{I_1(qb)}{q^3 I_1'(qb)}\,dk. \tag{2.2.7}$$

In the gap, $|z|<d$, the integrals in these expressions can be converted into seems devoid of Bessel functions by the method of contour integration used in Section 1.

Near $q=0(k=\pm\omega/c)$ we observe that $I_1(qb)\approx qb/2$, and $I_1'(qb)\approx 1/2$, so that both integrals have poles at $K=\pm\omega/c$. However, these poles do not exist in the expression for $B_\theta^{TM}+B_\theta^{TE}$, so we ignore them in evaluating each integral separately. The contour integration of B_θ^{TM} progresses just as in Section 1. To evaluate the pole at $k=0$ we note that

$$I_1'(i\omega b/c) = \frac{1}{i}\frac{dI_1(i\omega b/c)}{d(\omega b/c)} = J_1'(\omega b/c).$$

We have previously defined $\nu_s^2=\beta_s^2-(\omega/c)^2$, with $J_0(\beta_s b)=0$. We use a new symbol ε_s given by

$$\varepsilon_s^2=\beta_{1s}^2-(\omega/c)^2, \tag{2.2.8}$$

with $J_1(\beta_{1s}b)=0$. In terms of this quantity, the contour integration B_θ^{TM} yields

$$B_\theta^{TM}(\text{gap}) = -\frac{\omega}{c}A_1\cos\theta e^{i\omega t}\left\{\frac{J_1'(\omega b/c)}{J_1(\omega b/c)}+\frac{2\omega}{cb}\sum_{\beta_{1s}}\frac{e^{-\varepsilon_s d}\cosh\varepsilon_s z}{\varepsilon_s^2}\right\}. \tag{2.2.9}$$

The contour integration of B_θ^{TE} requires evaluation of $dI_1'(qb)/dk$ to evaluate the residues at $I_1'(qb)=0$. At these poles $q_s=i\rho_s$, where $J_1'(\rho_s b)=0$, and $k=\pm i\mu_s$, where

$$\mu_s^2=\rho_s^2-(\omega/c)^2. \tag{2.2.10}$$

At these poles we have $dI_1'(qb)/dk=(kb/q)I_1''(qb)$, where double prime indicates the second derivative with respect to argument. From Bessel's equation with $I_1'=0$, we have

$$I_1''(qb)=\left[1+\frac{1}{(qb)^2}\right]I_1(qb).$$

The result of the contour integration of B_θ^{TE} is

$$B_\theta^{TE}(\text{gap}) = \frac{2A_1}{b}\cos\theta e^{i\omega t}\sum_{\rho_s}\frac{e^{-\mu_s d}\cosh\mu_s z}{[\rho_s^2 b^2-1]}. \tag{2.2.11}$$

In the box, we again neglect the axial dependence of the field components and write

$$A_z^{II}=A_1\frac{G_1(\omega r/c)}{G_1(\omega b/c)}\cos\theta e^{i\omega t}, \tag{2.2.12}$$

with the function G_1 given by

$$G_1(\omega r/c)=J_1(\omega r/c)+C_1N_1(\omega r/c). \tag{2.2.13}$$

and

$$C_1 = \frac{[i(Z_s/Z_0)J_1'(\omega R/c) - J_1(\omega R/c)]}{[N_1(\omega R/c) - i(Z_s/Z_0)N_1'(\omega R/c)]}. \tag{2.2.14}$$

In the box, we have

$$B_\theta^{II} = -A_1 \frac{\omega}{c} \frac{G_1'(\omega r/c)}{G_1(\omega b/c)} \cos\theta e^{i\omega t}. \tag{2.2.15}$$

Equation (2.2.12) insures the continuity of E_z and B_r in the gap.

We insert Eqs. (2.2.9), (2.2.11), and (2.2.15) together with Eq. (B8) into Eq. (2.2.5) and average over the gap to obtain the expression for A_1 vs. ω. Because we are calculating the transverse magnetic field, we write

$$\frac{A_1}{b} = \frac{4I\xi}{cb^2} \frac{\sin(\omega d/v)}{(\omega d/v)} \frac{1}{H_1}, \tag{2.2.16}$$

with

$$H_1 = \left(\frac{\omega b}{c}\right)\left[\frac{J_1'(\omega b/c)}{J_1(\omega b/c)} - \frac{G_1'(\omega b/c)}{G_1(\omega bc)}\right] - \frac{1}{d}\sum_{\rho_s} \frac{(1-e^{-2\mu_s d})}{\mu_s[\rho_s^2 b^2 - 1]} + \frac{1}{d}\left(\frac{\omega}{c}\right)^2 \sum_{\beta_{1s}} \frac{(1-e^{-2\varepsilon_s d})}{\varepsilon_s^3}. \tag{2.2.17}$$

2.3. *Determination Z_t and Q for TM_{1n0} Modes*

We calculate the change in transverse momentum, Δp_x of a particle crossing the cell in the same manner as the change in energy was calculated in Section 1.4. The force F_x in the x direction is

$$\begin{aligned} F_x &= e[E_x - (v/c)B_y], \\ &= -e\left[\frac{1}{c}\frac{\partial A_x}{\partial t} + \frac{v}{c}\frac{\partial A_x}{\partial z} - \frac{v}{c}\frac{\partial A_z}{\partial x}\right]. \end{aligned} \tag{2.3.1}$$

The operator on A_x is the total time derivative along the particle path, and integrates to zero, so that

$$\Delta p_x = \frac{e}{c}\int \frac{\partial A_z}{\partial x}\, dz, \tag{2.3.2}$$

where again the integral is taken along the particle path $z = v(t - t_0)$. (The radial position of the particle is assumed constant while the particle crosses the cell.) We will use Eq. (2.2.2) and calculate $\int A_z\, dz$ as in Section 1.4 above, then perform $\partial/\partial x$ of the result. We obtain

$$\int A_z\, dz = 2\, dA_1 \cos\theta e^{i\omega t_0} \frac{\sin(\omega d/v)}{(\omega d/v)} \frac{I_1(gr)}{I_1(gb)}. \tag{2.3.3}$$

Again, for relativistic particles we use $I_1(gr) = gr/2$ and $I_1(gb) = gb/2$. Noting that

$\partial/\partial x = \partial/\partial(r\cos\theta)$ we have

$$\int (\partial A_z/\partial x)\, dz = \frac{2\, dA_1}{b}\, e^{i\omega t_0} \frac{\sin(\omega d/v)}{(\omega d/v)}. \tag{2.3.4}$$

We include the additional transit-time factor and introduce the quantity A_1^e by

$$A_1^e = \frac{\sin(\omega d/v)}{(\omega d/v)} A_1. \tag{2.3.5}$$

We numerically determine the quantity $P_1(\omega)$ defined by

$$P_1(\omega) = \frac{\sin^2(\omega d/v)}{(\omega d/v)^2} \frac{1}{H_1}$$

$$= \frac{cb}{4I\xi} A_1^e. \tag{2.3.6}$$

Graphs of Im $P_1(\omega)$ vs $\omega R/c$ are shown in Figs. 6, 7, and 8 for $Z_s/Z_0 = 1, 2$, and 3 respectively. The curves extend to $\omega R/c = 6.58$, which corresponds to the cutoff frequency of the beam pipe given by $\omega b/c = 1.841$. For $b = 7.5$ cm, the cutoff frequency is 1163 MHz.

For $Z_s/Z_0 = 2$ and 3, two peaks occur at $\omega R/c = 1.8$ and 5, corresponding to frequencies of 318 MHz and 884 MHz respectively. The model is therefore not quite as successful in predicting the frequencies of the TM_{110} and TM_{130} modes as it is in predicting the frequency of the TM_{030} mode. For $Z_s = Z_0$, there is only one peak, again at a lower frequency.

We evaluate Z_t and Q from the graphs of Im P_1 and Eq. (2.1.3). At resonance, Eq. (2.1.3) yields $V_t = -i\omega_0 Z_t I\xi/c$, and from Eq. (2.3.4), we have $V_t = 2\, dA_1^e/b$, so that

$$Z_t I\xi = -2d(c/\omega_0 b)\ \text{Im}\ A_1^e(\omega_0), \tag{2.3.7}$$

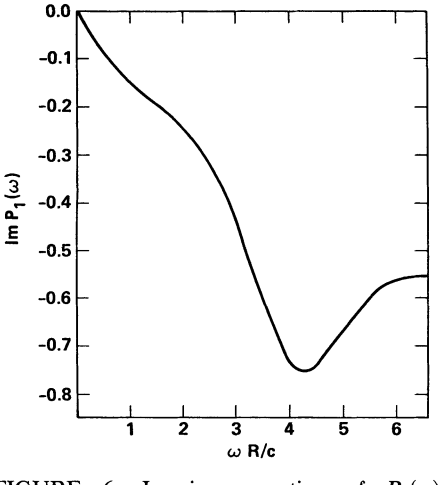

FIGURE 6. Imaginary portion of $P_1(\omega)$ defined by Eq. (2.3.6) vs $\omega R/c$ for $Z_s = Z_0$.

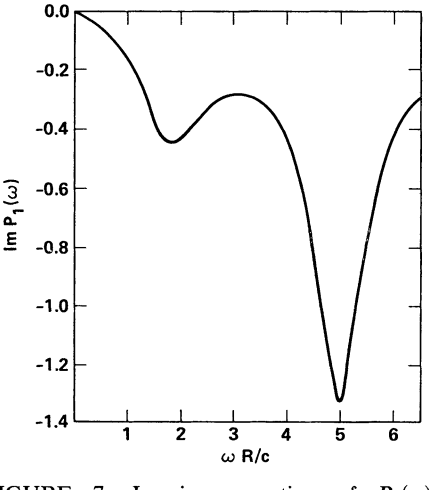

FIGURE 7. Imaginary portion of $P_1(\omega)$ defined by Eq. (2.3.6) vs $\omega R/c$ for $Z_s = 2Z_0$.

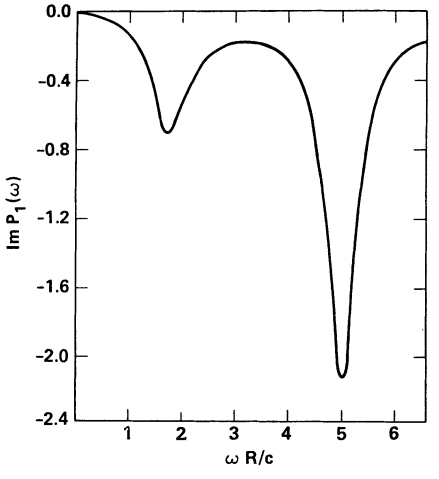

FIGURE 8. Imaginary portion of $P_1(\omega)$ defined by Eq. (2.3.6) vs $\omega R/c$ for $Z_s = 3Z_0$.

Employing Eq. (2.3.6) we have

$$Z_t = -\frac{8d}{cb}\left(\frac{c}{\omega_0 b}\right) \text{Im } P_1(\omega_0).$$

Dividing by $Z_0 = 4\pi/c$ in these units, we have

$$\frac{Z_t}{Z_0} = -\frac{2d}{\pi b}\left(\frac{c}{\omega_0 b}\right) \text{Im } P_1(\omega_0). \tag{2.3.8}$$

From Figs. 7 and 8, we find $Z_t = 38\ \Omega$ for $Z_s = 2Z_0$ and $Z_t = 62\ \Omega$ for $Z_s = 3Z_0$. The Q values are estimated from the graphs and Eq. (1.4.10) with $P(\omega)$ replaced by $P_1(\omega)$. We find $Q = 4.3$ for $Z_s = 2Z_0$ and $Q = 7.6$ for $Z_s = 3Z_0$. It is not possible to obtain a Q value for $Z_s = Z_0$, because our technique yields values less than unity. We notice that the value of Z_t/Q is larger for $Z_s = 2Z_0$ than for $Z_s = 3Z_0$. The choice of values of Z_s/Z_0 in our model was empirical. The behavior of the transverse motion of the beam in ATA (before laser guiding was implemented) was consistent with a coupling impedance of about 30 to 35 Ω and a Q value of 4 to 6. A significant result is agreement between values of Z_t and Q measured in cold tests and values determined from the behavior of the beam in the Accelerator. Furthermore, our model demonstrates that the damping mechanisms employed in the cell are about as good as one can do.

REFERENCES

1. V. K. Neil, L. S. Hall, and R. K. Cooper, *Part. Acc.* **9** 213, (1979).
2. D. L. Birx, "Microwave Measurements of the ETA Accelerating Cavity," LLNL Report UCID-18582, March 12, 1980.
3. D. L. Birx, "Reduction of the Beam Breakup Mode Q Values in the ETA/ATA Accelerating Cells," LLNL Report UCID-18630, May 20, 1980.
4. R. J. Briggs, Proc. of 1981 Part. Acc. Conf., *IEEE Trans. Nucl. Sci.* Vol. NS-28, No. 3, p. 3360 (1981).
5. W. E. Martin, G. J. Caporaso, W. M. Fawley, D. Prosnitz and A. G. Cole, Phys. Rev. Letters. *54*, 685 (1985).

APPENDIX A

We consider a beam of particles with charge and axial current densities ρ and $j(=\rho v)$ respectively that are radially uniform out to radius $r=a$ and zero beyond. The axial (z) and time-dependence of all quantities is $e^{i\omega(t-z/v)}$. The electric and magnetic field components arising from these sources are E_r, E_z, B_θ. These field components obey Maxwell's equations in cylindrical coordinates. In Gaussian units we have

$$\nabla \times \mathbf{E} = -\frac{1}{c}\frac{\partial \mathbf{B}}{\partial t}, \tag{A1}$$

$$\nabla \times \mathbf{B} = \frac{1}{c}\frac{\partial \mathbf{E}}{\partial t} + \frac{4\pi \mathbf{j}}{c}, \tag{A2}$$

$$\nabla \cdot \mathbf{E} = 4\pi p, \tag{A3}$$

$$\nabla \cdot \mathbf{B} = 0. \tag{A4}$$

In the usual fashion, we take the curl of Eq. (A1) and employ Eqs. (A2) and (A3) to obtain the equation for E_z, which is

$$\nabla^2 E_z = \frac{1}{c^2}\frac{\partial^2 E_z}{\partial t^2} + \frac{4\pi}{c^2}\frac{\partial j}{\partial t} + 4\pi \frac{\partial \rho}{\partial z}. \tag{A5}$$

The factor $\exp i\omega[t-(z/v)]$ is understood to be appended. With the above relations, we reduce Eq. (A5) to the form

$$\frac{1}{r}\frac{\partial}{\partial r}\left(r\frac{dE_z}{\partial r}\right) - g^2 E_z = -\frac{4\pi i\omega\rho}{\gamma^2 v}, \tag{A6}$$

in which $\gamma^{-2} = 1-\beta^2$, $\beta = v/c$, and

$$g = \omega/v\gamma. \tag{A7}$$

Equation (A6) is valid for $r<a$. For $a<r<b$, E_z obeys the same equation, but with the right hand side equal to zero.

The solution to Eq. (A6) is easily obtained, and from that solution we may obtain expressions for E_r and B_ϕ. The electric field in the region $r<a$ is given by

$$\mathbf{E} = E_i[I_1(gr)\hat{r} - (i/\gamma)I_0(gr)\hat{z}] + 4\pi i(v\rho/\omega)\hat{z}. \tag{A8}$$

In this expression I_n is the modified Bessel function of the first kind of order n and E_i is a constant to be evaluated. In the region $a<r<b$ we have

$$\mathbf{E} = E_0[F'(gr)\hat{r} - (i/\gamma)F(gr)\hat{z}]. \tag{A9}$$

In this expression E_0 is a constant to be evaluated and

$$F(gr) = K_0(gb)I_0(gr) - I_0(gb)K_0(gr), \tag{A10}$$

in which K_n is the modified Bessel function of the second kind of order n. The form of F insures that $E_z = 0$ at the conducting pipe wall, $r=b$. In both regions we have

$$B_\theta = \beta E_r. \tag{A11}$$

The constants E_i and E_0 are found by the continuity of E_r and E_z at $r = a$. The Wronskian relation,

$$I_0(x)K_0'(x) - I_0'(x)K_0(x) = -(1/x),$$

and a little algebra is involved in this process. The results are

$$E_0 = \frac{4\pi v\gamma\rho}{\omega} ga \frac{I_1(ga)}{I_0(gb)}, \tag{A12}$$

and

$$E_i = E_0 F'(ga)/I_1(ga). \tag{A13}$$

The magnetic field B_θ at the wall is therefore

$$B_\theta(r = b) = 4\pi\beta\rho a I_1(ga)/gbI_0(gb). \tag{A14}$$

The axial wall current $K = -cB_\theta/4\pi$. In terms of the total beam current $I = \pi\rho v a^2$, we have

$$K = -\frac{I}{\pi} \frac{I_1(ga)}{gabI_0(gb)}. \tag{A15}$$

For relativistic particles ga and $gb \ll 1$, $I_0(gb) = 1$ and $I_1(ga) = ga/2$. With these approximations, and with the exponential factor explicit, we have

$$K = -(I/2\pi b)e^{i\omega[t-(z/v)]}. \tag{A16}$$

APPENDIX B

We consider a beam of particles of radius $r = a$ carrying current I in the positive z direction. The beam is on axis inside a conducting pipe of radius b. The configuration of wall currents is not sensitive to the distribution of current within the beam, so we may take the current density to be uniform for $r < a$ and zero for $r > a$. On this beam we impose rigid transverse oscillations in the x direction with a displacement $\mathbf{D}$ given by

$$\mathbf{D} = e^{i\omega\tau}\hat{x}, \tag{B1}$$

with $\tau = t - (z/v)$.

The current that gives rise to the fields of interest is the surface current K_b in the z direction located at $r = a$ and given by

$$K_b = (I\xi/\pi a^2)\cos\theta e^{i\omega\tau}. \tag{B2}$$

The axial component of the vector potential resulting from this current source obeys Eq. (2.2.1). We introduce the quantities g and F_1 by the definitions $g \equiv \omega/v\gamma$,

$$F_1(gr) = \begin{cases} [K_1(gb)I_1(ga) - I_1(gb)K_1(ga)]I_1(gr), & r < a, \\ [K_1(gb)I_1(gr) - I_1(gb)K_1(gr)]I_1(ga), & a < r < b. \end{cases} \tag{B3}$$

In terms of these quantities the vector potential satisfying Eq. (2.2.1) and

$\nabla \cdot \mathbf{A} = 0$ is of the form

$$\mathbf{A} = Ne^{i\omega\tau}\left\{\cos\theta F_1'\hat{r} - \sin\theta\frac{F_1}{gr}\hat{\theta} - \frac{i}{\gamma}\cos\theta F_1\hat{z}\right\}, \tag{B4}$$

in which prime indicates $d/d(gr)$ and N is a constant to be found from the discontinuity in B_θ at $r = a$. We note that the vector potential provides no axial magnetic field.

From $B_\theta = (\partial A_r/\partial z) - (\partial A_z/\partial r)$ we have

$$B_\theta = -\frac{i\omega v}{c^2} Ne^{i\omega\tau}\cos\theta F_1'(gr). \tag{B5}$$

The function F_1 is continuous at $r = a$. We employ the Wronskian, $K_1(x)I_1'(x) - K_1'(x)I_1(x) = 1/x$, to evaluate the discontinuity in F_1' at $r = a$, and find $F_1'(ga)^+ - F_1'(ga)^- = I_1(gb)/ga$.

From the condition $B_\theta^+ - B_\theta^- = 4\pi K_b/c$ we obtain

$$B_\theta = \frac{4\pi K_b ga}{cI_1(gb)} F_1'(gr), \tag{B6}$$

with K_b given by Eq. (B2). To evaluate B_θ at the conducting wall $r = b$ we again employ the Wronskian to obtain $F_1'(gb) = I_1(ga)/gb$. The wall current K_t is in the axial direction and found from

$$4\pi K_t/c = -B_\theta(r = b),$$

which yields

$$K_t = -\frac{I\xi}{\pi ab}\left[\frac{I_1(ga)}{I_1(gb)}\right]\cos\theta e^{i\omega\tau}. \tag{B7}$$

For relativistic beams $gb \ll 1$ and we may use the approximate expression

$$K_t = -(I\xi/\pi b^2)\cos\theta e^{i\omega\tau}. \tag{B8}$$